Characterization of Rat Tail Tendon Material Properties

Aidan Boyne

Introduction

To fully understand the causes and potential treatments of tendon injuries, it is critical to first identify and describe their mechanical properties. Unlike bone, which can be reasonably described using linear elastic models, tendons require more complex mathematical descriptions such as viscoelastic and hyperelastic models to account for nonlinear sliding behavior between tendon components [7].

Functioning primarily to transmit force from the muscles to the skeleton, tendons are composed of collagen fibers arranged in bundles of increasing size [4]. This organization and the intrinsic properties of collagen (and to a smaller extent, elastin) result in a tissue specialized for one dimensional tensile force transfer and in some cases such as the Achilles tendon, energy storage and release. As a result, tendonous tissue is especially well suited for one dimensional tensile testing and numerical modeling [4].

In this report, several loading tests were applied to tendons taken from rat tails. Elasticity and viscosity parameters were then extrapolated from the data and used to construct several finite element model (FEM) simulations.

The loading tests applied to the rat tail tendons consisted of a creep test, cyclic loading test, and several tensile tests at different strain rates. These tests were chosen to investigate both the linear and nonlinear elastic and viscoelastic properties of the tendon including young's modulus, hysteresis, and creep behavior. Together, these parameters describe tendon behavior during both explosive and sustained motion.

Based on research by Herrick et. al. and the characteristics of common viscoelastic models (diagram 3) we hypothesized that the tendons would exhibit slightly increased stiffness and a correspondingly greater young's modulus at higher strain rates [2]. We also predicted that the toe region would show little if any change in length based on previous research by Ng et al. [6].

In the creep test, we hypothesized that displacement would slowly increase over time when a constant force was applied. Based on research by Shen et. al., we expected a time constant in the region of 50s-100s [7].

Finally, for the cyclic loading test, we hypothesized that the energy loss in a loading-unloading cycle would decrease as more loading cycles were completed based on previous research by Finni et. al. [1].

Experimental Lab

Methods

The tendons used in all of the loading tests were dissected out of a rat tail. Rat tail tendons in particular were chosen due to both availability and relatively consistent fibril length and cross-sectional area [3]. To isolate the tendons, the skin was first cut and pulled back to reveal the tendon fascicles surrounding the tail bone. Each fascicle was then carefully removed to avoid tissue damage and stored in the refrigerator under buffered saline solution to preserve the tissue until testing.

Before loading, the tendon fascicles were set out to reach room temperature. Six fascicles of similar length were then laid out and their ends were wrapped around wooden sticks and covered with a small piece of sandpaper to prevent slipping during the tests. These ends were then clamped into the vices of a KIP Instron 8511 tensile testing frame and measured as shown in diagram 1. During all steps of the preparation and testing process the fascicles were periodically wet with the saline buffer solution.

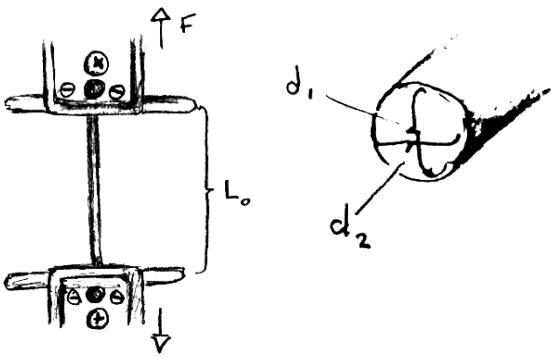

Diagram 1. A schematic illustrating the geometry of the tensile testing apparatus and fascicle bundle

First, the effect of tensile strain rate on the mechanical response of the tendons was investigated by stretching the sample until a force of 10N was detected. Three trials were conducted at displacement rates of 0.1mm/s, 1.0mm/s, and 10mm/s. The force-displacement data obtained was used to derive the stress-strain curve according to equations *(a)* and *(b)* in Diagram 2 under the assumption that the tendon possessed a circular cross-section. Using linear regression, a line of best fit was calculated for the elastic region of the graph. The young's modulus for each strain rate was taken as the slope of the line of best fit. Next, the toe region of the stress-strain curve was defined as the region to the left of the elastic region, and the maximum strain obtained during the toe region was recorded for comparison between the strain rates.

Next, to determine the viscoelastic creep behavior of the tendons, a sustained tensile load of 10N was applied for 2 minutes following an initial linear ramp up from 0 to 10N over 10 seconds. The displacement during the sustained load was recorded and combined with geometrical measurements to create a stress-strain curve using equations *(a)* and *(b)*. Finally, the elastic (E_i) and viscous (η) parameters in the Maxwell, Kelvin-Voigt, and Standard Linear Solid (SLS) viscoelastic material equations determined by fitting the stress-strain curve (brief derivations of the equations are shown in diagram 3). The fitting was accomplished via MATLAB optimization tool *fminsearch* which was used to minimize the root mean squared (rms) error

between the experimental data points and calculated values for each model. The time constant *t*, defined as the time when strain reached 63% of its asymptotic value, was also determined.

Lastly, tendon behavior under repeated loads was investigated due to its relevance for physiological motions such as walking and jogging. The tensile force exerted by the tendons was measured as they were stretched 1.1mm from a resting length of 22.86mm (about 5% strain) and relaxed 5 times over 11s. Next, the stress-strain curves were plotted, again using equations *(a)* and *(b)*. The area between the loading (upper) and unloading (lower) curves corresponding to cyclic energy loss (CEL) was calculated as the difference of the sum of stresses multiplied by strains from the loading and unloading curves via equation *(c)*.

Diagram 2. Equations used during stress-strain and hysteresis calculations

$$(a)\ \sigma = \frac{\mathrm{F}}{\mathrm{A}}\ \ where\ \ A = \pi\left(\frac{d_1 + d_2}{4}\right)^2$$

$$(b)\ \epsilon = \frac{\Delta l}{l_0}$$

$$(c)\ CEL = \sum \sigma_{load} * \epsilon_{load} - \sum \sigma_{unload} * \epsilon_{unload}$$

Results

The results of the tensile strain rate test are presented in table 1. Increasing the strain rate resulted in a greater measured young's modulus tough the magnitude of the change was rather small: increasing the strain rate 100x resulted in an 18.1% greater young's modulus. Maximum stress observed similarly increased by 15.6% over the three trials. The toe region showed no significant change in length and the tendons began exhibiting linear-elastic behavior at around 0.9% strain in all of the trials as shown in table 1.

The strain data obtained from the creep test is shown in figure 1. Additionally, the strains calculated using the viscoelastic models are displayed over the experimental data. Out of all the models, the SLS preformed the best with a rms error of 7.14%. The Kelvin-Voigt model also captured the shape of the experimental data

Diagram 3. Viscoelastic model equations (bolded) and abbreviated derivations. All models were derived from initial equations based on the spring and dashpot equations. Stress (σ) was then set to σ_0 and $\frac{d\sigma}{dt}$ was set to zero. The resulting equations were solved for strain (ϵ) and differential equations were solved in terms of elastic (E_i) and viscous (η) parameters.

Maxwell Model

$$\frac{d\epsilon}{dt} = \frac{d}{dt}\left(\frac{\sigma}{E}\right) + \frac{\sigma}{\eta}$$

$$\frac{d\epsilon}{dt} = \frac{\sigma}{\eta}$$

$$\boldsymbol{\epsilon = \sigma_0\left(\frac{1}{\eta}t + \frac{1}{E}\right)}$$

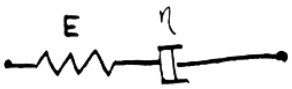

Kelvin-Voigt Model

$$\sigma = E\epsilon + \eta\left(\frac{d\epsilon}{dt}\right)$$

$$\frac{d\epsilon}{dt} = \frac{\sigma_0}{\eta} - \frac{E\epsilon}{\eta}$$

$$\boldsymbol{\epsilon = \frac{\sigma_0}{E}\left(1 - e^{\left(-\frac{E}{\eta}\right)t}\right)}$$

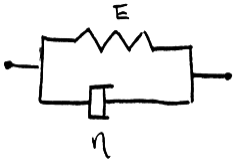

Standard Linear Solid (SLS) Model

$$\sigma = E_2\left(\epsilon - \frac{\sigma}{E_1}\right) + \frac{d}{dt}\left(\epsilon - \frac{\sigma}{E_1}\right)$$

$$\frac{d\epsilon}{dt} + \frac{E_2}{\eta}\epsilon = \frac{\sigma}{\eta}\left(\frac{E_1 + E_2}{E_1}\right)$$

$$\boldsymbol{\epsilon = -\frac{\sigma_0}{E_2}e^{\left(-\frac{E_2}{\eta}\right)t} + \sigma_0\left(\frac{E_1 + E_2}{E_1 E_2}\right)}$$

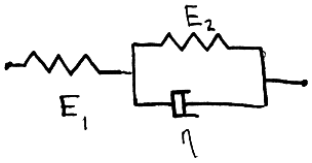

Table 1. Summarized data for tensile strain rate trials. Toe region length was defined as the strain at which the linear approximation intersected experimental data

Strain Rate	Youngs Modulus (MPa)	Toe region length (%)	Maximum Stress (MPa)
0.10 mm/s	176.3	0.89	4.54
1.0 mm/s	205.1	0.92	4.67
10.0 mm/s	208.2	0.92	5.25

Figure 1. Experimental strain-time data (grey) plotted with calculated viscoelastic models.

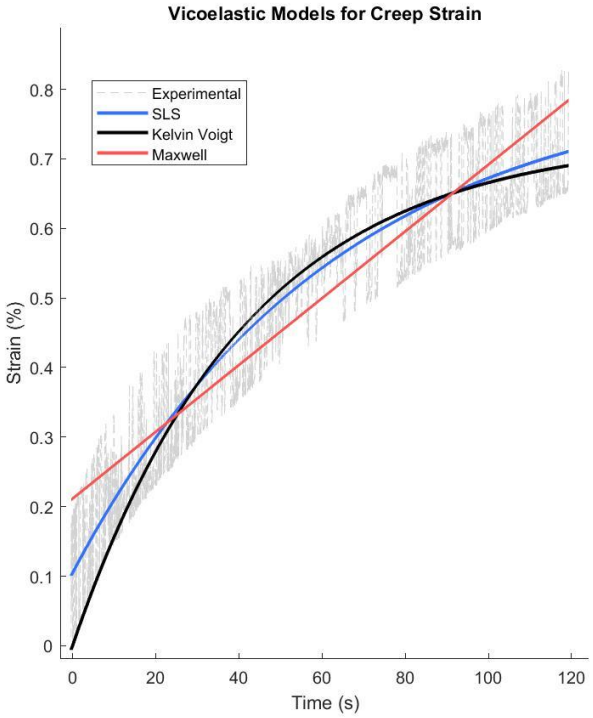

and had a rms error of 7.82%. The Maxwell model preformed the worst with a rms error of 8.52%. Lastly, the time constant for the tendon under 10N of constant force was t = 46.96s, calculated using strain values calculated via the SLS model.

The force-displacement data and calculated CEL for each cycle during the cyclic loading test is shown in figure 2. Over the course of the trial, CEL decreased by 36.3% with the greatest drop between consecutive cycles (15.6%) occurring between cycle 1 and cycle 2. Peak force experienced during each cycle also decreased to, albeit to a lesser extent: 8.6% over the course of the trial and 3.1% between cycle 1 and cycle 2.

Figure 2. (Left) Loading and unloading force-displacement curves for the tendon under 5 loading cycles to 1.1mm. Top curves for each color correspond to loading and bottom curves to unloading. (Right) Energy loss for each cycle corresponding to area between the loading and unloading curves.

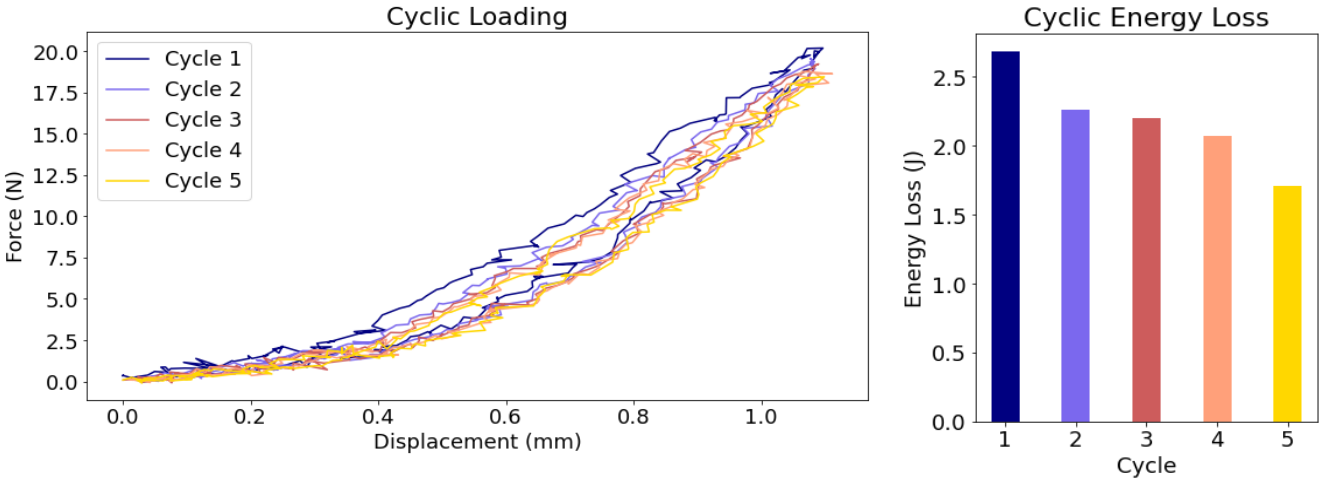

Discussion

Overall, the tendon behavior was consistent with the predictions made in the hypothesis for the various tests and all of the parameters we set out to measure in the hypotheses were successfully measured. In the strain tests, the ~18% increase in young's modulus over the three trials is consistent with data found in in-vivo horse tendon trials by Herrick et. al. [2]. The actual values, however, are smaller than those in literature – for example compare the calculated value of 205.1MPa in the 1.0mm/s trial to Herrick et. al.'s average value of 827MPa [2]. A likely reason for this discrepancy is the swelling of tendon fascicles during storage under the buffer solution. This swelling has been shown to have a negligible effect on the force displacement data but the accompanying increase cross sectional area could result in far lower calculated stress values [3]. This idea is supported by the fact a study using a similar isolated fascicle testing procedure also recorded lower values of about 150MPa [7].

As a result of this increased cross-sectional area, lower stresses would be associated with the same strain, at least partially explaining the smaller values for young's modulus seen here. The toe region's lack of change, though expected, can still shine light on the crimp structure seen in collagen fibrils (see diagram 4) [8]. A possible explanation for the uniformity of the toe region is that the "de-crimping" of collagen is independent of strain rate, though further investigation such as microscopy would be necessary to confirm this hypothesis.

The shape of the creep data was quite similar to that in literature though the time constant was somewhat smaller (46.96s vs. ~100s) [7]. It is important to note that the rapid fluctuations in recorded strain resulting in a 'fat' curve for the experimental data are a result of the testing apparatus attempting to maintain a constant 10N load. Consequently, the rms error of all of the models is likely greater than it would be if the apparatus could perfectly maintain the load. Additionally, it appears that the tendon was not able to fully reach a steady-state strain during the two minutes of the trial which could partially explain the lower-than-hypothesized time constant. As for the mathematical models, it is obvious that the Maxwell equation is unable to capture the nonlinear creep behavior of the tendon. Both the SLS and Kelvin-Voigt, however, provide reasonable approximations. While the SLS has the advantage of lower rms

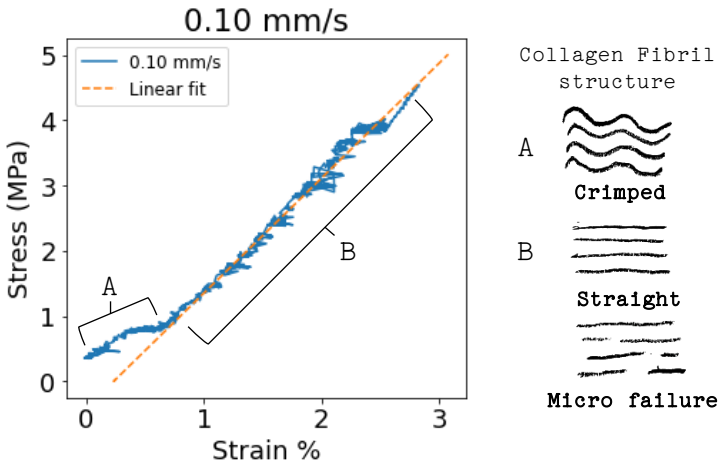

Diagram 4. Example stress-strain curve from 0.10mm/s strain rate test. Depiction of collagen fibril structure at each region is shown to the right. *(Note micro failure is not shown in the example curve and typically occurs at 10-15% strain [5].)*

error, it also predicts unrealistic behavior at the beginning of the strain-time curve (for example, a strain of 0.1% at 0 seconds), so both models should be taken into consideration for future applications [7]. The general numerical modelling optimization could likely be extended human tendons as well as all three models derived via rms error minimization were stable with regard to initial parameter estimates as long as they were in a reasonable range.

Lastly, the cyclic loading tests exhibited decreasing energy loss as hypothesized. Interestingly, the hysteresis data obtained from the cyclic loading tests was very similar to data from recent in-vivo human studies conducted using ultrasound imaging [1]. After converting the data from absolute energy loss (J) to relative energy loss to total energy under the curve (%), the rat tail tendons were found to have a maximum and minimum hysteresis of 32.4% and 24.8% on cycles 1 and 5 respectively. Compare this to the ultrasound studies which recorded hysteresis values from 36% to 7% in human Achilles' tendons. In-vitro animal studies, however, arrived at much lower hysteresis values ranging from 10.7% to 4.8% [1]. Notably, the animal studies all included extensive preconditioning, often subjecting the tendon to hundreds of loading cycles before recording hysteresis values. Future testing on the rat-tail tendons over several thousand cycles would be useful and could paint a fuller picture of energy loss over extended periods of time reflecting activities such as long distance running or cycling. When designing this or other future tests, it is important to consider the cost and ethical implications of animal testing. These can often be avoided using numerical methods such as those introduced in the following section.

Numerical Lab

Methods

Using data taken from a similar series of experiments run on rat-tail tendons, a FEM was constructed to compare the accuracy of various material models. First, a simple linear elastic model using the young's modulus of 326MPa determined from a 1mm/s tensile strain test was constructed. The stress-strain data was also used to fit several hyperelastic material models: a Neo-Hookean model with a residual of 96.18 and 1st, 2nd, and 3rd order Ogden models which had residuals of 15.93. 10.63, and 7.81 respectively. The 3rd order Ogden model was chosen for the hyperelastic simulations as it had the lowest residual. A similar procedure was used to fit viscoelastic 1st, 2nd, and 3rd order Prony models to the creep data using an assumed Poisson's ratio of 0.30. The resulting models had residuals of 2.63e-4,1.70e-5, and 5.09e-6 respectively. The 3rd order Prony model was selected and combined with the 3rd order Ogden model to create a hyper-viscoelastic model used in the simulations.

Once the material model parameters were fitted to the experimental data, a simple 2-D rectangle with dimensions 59.80mmx1.39mm was created and meshed using 12 elements to represent the tendon. The bottom nodes were restricted in all dimensions of movement to simulate the clamp of the testing apparatus and a 3.05mm displacement was applied to the top nodes (see diagram 5). Three different rates of displacement - 0.002 mm/s (Slow), 1 mm/s (Normal), and 500 mm/s (Rapid) – were applied to the tendon mesh under each of the

3 selected material models for a total of 9 simulated tests.

Finally, the force-displacement data for each of the trials was compared to the 1mm/s experimental tensile data for both validation and to examine the effect of strain rates. Both the experimental and simulated test data are shown in figure 3.

Results

Graphs of force-displacement data for the simulated tensile tests under the discussed material models and strain rates are presented in figure 3. Experimental data is shown for comparison. The rms error and parameter values for each model at a strain rate of 1.0 mm/s (corresponding to that of the experiment) were calculated and are presented in table 2 along with the predicted and experimental maximum stress and strain values.

Notably, the linear model has over twenty times the rms error as the hyperelastic and hyper-viscoelastic models, which had nearly identical error values. The maximum predicted stress values for the hyperelastic and hyper-viscoelastic models were also similar and underestimated the experimental maximum stress by around 7% while the linear elastic model overshot by over 44%.

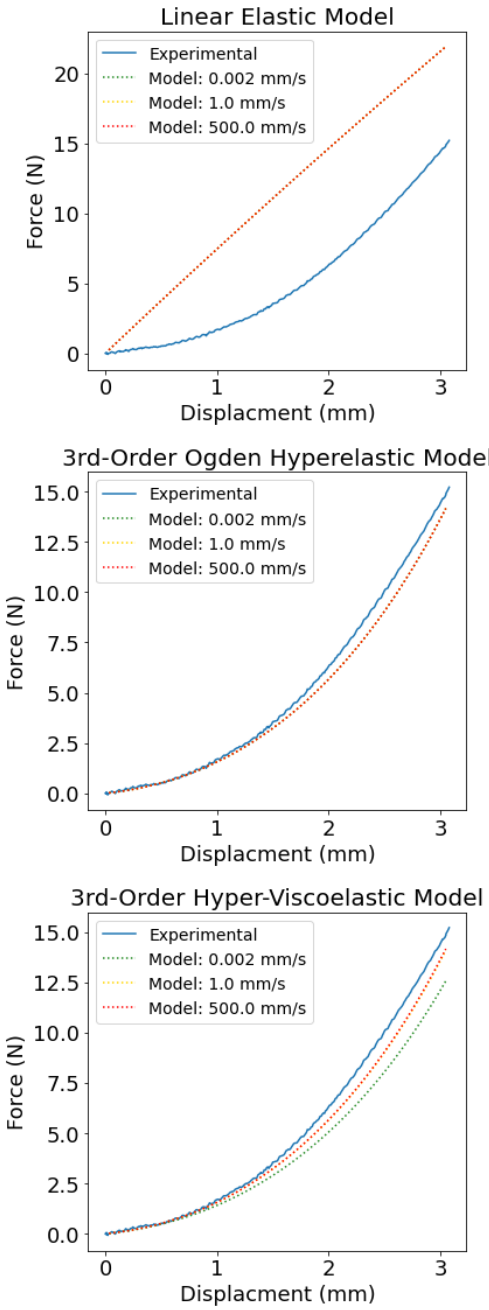

Figure 3. (Above) Comparison of material models and strain rates used in FEM simulations. Note that only the Hyper-Viscoelastic Model shows any strain rate dependence.

Diagram 5. (Below) Depiction of FEM geometry, boundary conditions, and loading direction

Table 2. Error values, maximum stresses, and parameter values for the chosen material models. Parameters μ_i, α_i, define the shear modulus while d defines the bulk modulus.

Material Model	Linear Elastic	3rd Order Ogden	3rd Order Hyper-Viscoelastic	Experimental
Max Stress (MPa)	14.62	9.44	9.39	10.15
RMS Error (%)	62.68	3.73	3.93	-
Young's Modulus (MPa)	326	-	-	326
Poisson's Ratio	0.30	-	-	0.30
μ_1 (MPa), α_1	-	-3149.22, 0.831	8.5496,1.501	-
μ_2 (MPa), α_2	-	0.728, 46.534	17.013, 0.845	-
μ_3 (MPa), α_3	-	945.29, 2.748	1.799, 2.802	-
d (m^2/N)	-	-	125.00	-

Discussion

As expected, the linear elastic model was unable to capture the tendon behavior and should only be used as an extremely rough approximation before applying more accurate material models. Both the 3rd order Ogden hyperelastic and 3rd order hyper-viscoelastic models (based on the 3rd order Prony Series), however, provided a reasonable approximation of tendon behavior with similar rms error to existing numerical models [7].

If strain rate or creep behavior are a concern, the hyper-viscoelastic model is the most appropriate choice as no other model showed any response to the speed of deformation. This is because hyperelastic equations have no strain rate dependence, so viscoelastic equations are necessary to capture time-dependent behavior. If time dependent behavior is unimportant to the particular experiment, however, the Ogden hyperelastic model is likely a sufficient and less computationally expensive alternative. If the region of interest is very small and lies past the toe region, even linear models may give some insight into tendon behavior.

With regard to ethics, finite element models provide an animal free and rapid way to test a huge number of possible loading conditions. In-vivo ultrasonography is another promising method to measure tendon properties without harming laboratory animals, and has shown some success in recent human studies.

Discussion

Overall, both experimental and numerical results emphasize the nonlinear nature of tendon biomechanics. In stark contrast to the biomechanics of bone tissue, time plays a significant role in a tendon's response to both rapid and extended forces [2]. Although both tissues are comprised of repeating substructures (haversian canals and fibril bundles in bone and tendon respectively), bone lacks significant internal movement. Modeling tendons is also complicated by crimps in the collagen microstructure not seen in bone [8]. These differences reflect the contrasting yet complementary purposes of tendon and bone tissue: tendons must be flexible and have high tensile strength to transmit muscle force to the bone, which must be rigid and strong in compression to use this force to move the body.

As tendon is such a mechanically complicated material, an abundance of experimental tests is needed to accurately determine its properties [3]. Experimental tests, however, are often costly and usually require animal

samples. As discussed previously, numerical methods such as finite element modeling are one attractive way around these problems. Numerical methods have the added benefit of being significantly faster, more scalable, and easier to tweak than physical experiments. As such, they are well suited to research where large amounts of data under many conditions are required. The importance of experimental evidence to construct and validate these models, however, is undeniable, and it is unlikely that we can completely replace physical testing.

Although this research focused on the tendons of a rat tail, the results are largely applicable to human tendons as well. Of course, there are some subtle differences between the two, but the composition and organization of rat tail and human tendons are remarkably similar [3]. Furthermore, unlike bone which has a more complex internal architecture that restructures in response to stress, tendon tissue is organized in the same way throughout the body in both rats and humans [3]. It follows that the mechanics of the two should mirror one another. This was confirmed at least in the case of cyclic loading, where the results of the rat tendon testing were nearly identical to that of ultrasonography studies of the human Achilles tendon [1].

To conclude, the results of this study provide a broad but by no means comprehensive look into the material properties of tendon tissue. Further experimental tests, both to obtain larger sample sizes and to measure behavior under more extreme or prolonged loading are warranted to provide data for more accurate numerical models. Microimaging during these experimental tests would also be an interesting area for further research to confirm the micro and nano-scale interactions responsible for the behavior observed. Altogether, though, the data from this and other studies gives us a solid understanding of how tendons work can help guide treatment of tendon injuries.

References

[1] Finni T., Peltonen J., Stenroth L., Cronin N.J. *Viewpoint: On the hysteresis in the human Achilles tendon.* Journal of Applied Physiology. Vol.114(1), 2013, pp. 515-517

[2] Herrick W.C., Kingsbury H.B., Lou D.Y.S. *A Study of the Normal Range of Strain, Strain Rate, and Stiffness of Tendon.* Journal of Biomedical Materials Research. Vol.12(1) 1978, pp. 877-894.

[3] Ker R.F., *Mechanics of tendon, from an engineering perspective*, International Journal of Fatigue. Vol.29(6), 2007, pp. 1001-1009.

[4] Kirkendall DT, Garrett WE. *Function and biomechanics of tendons*. Scandinavian Journal of Medical Science and Sports. Vol.7(2), 1997, pp. 62-66.

[5] LaCroix A.S., Duenwald-Kuehl S.E., Lakes R.S., Vanderby R. Jr. *Relationship between tendon stiffness and failure: a metaanalysis.* Journal of Applied Physiology. Vol.115(1) 2013, pp. 43-51.

[6] Ng BH, Chou SM, Lim BH, Chong A. *Strain rate effect on the failure properties of tendons*. Proceedings of Institute of Mechanical Engineering. Vol.218(3), 2004, pp. 203-206.

[7] Shen, Z. L., Kahn, H., Ballarini, R., Eppell, S. J. *Viscoelastic properties of isolated collagen fibrils*. Biophysical journal. Vol.100(12), 2001, pp. 3008–3015.

[8] Shim V, Fernandez J, Besier T, Hunter P. *Investigation of the role of crimps in collagen fibers in tendon with a microstructurally based finite element model.* Annual International Conference IEEE English Medical Biology Society. 2012, pp. 4871-4874.